

Unbiased roughness measurements: Subtracting out SEM effects, part 2

Gian F. Lorusso, Vito Rutigliani, Frieda Van Roey, and Chris A. Mack

Citation: *Journal of Vacuum Science & Technology B* **36**, 06J503 (2018); doi: 10.1116/1.5046477

View online: <https://doi.org/10.1116/1.5046477>

View Table of Contents: <http://avs.scitation.org/toc/jvb/36/6>

Published by the [American Vacuum Society](#)

HIDEN
ANALYTICAL

Instruments for Advanced Science

Contact Hiden Analytical for further details:

W www.HidenAnalytical.com

E info@hiden.co.uk

CLICK TO VIEW our product catalogue



Gas Analysis

- ▶ dynamic measurement of reaction gas streams
- ▶ catalysis and thermal analysis
- ▶ molecular beam studies
- ▶ dissolved species probes
- ▶ fermentation, environmental and ecological studies



Surface Science

- ▶ UHV TPD
- ▶ SIMS
- ▶ end point detection in ion beam etch
- ▶ elemental imaging - surface mapping



Plasma Diagnostics

- ▶ plasma source characterization
- ▶ etch and deposition process reaction kinetic studies
- ▶ analysis of neutral and radical species



Vacuum Analysis

- ▶ partial pressure measurement and control of process gases
- ▶ reactive sputter process control
- ▶ vacuum diagnostics
- ▶ vacuum coating process monitoring

Unbiased roughness measurements: Subtracting out SEM effects, part 2

Gian F. Lorusso,¹ Vito Rutigliani,¹ Frieda Van Roey,¹ and Chris A. Mack^{2,a)}

¹IMEC, Kapeldreef 75, B-3001 Leuven, Belgium

²Fractilia, LLC, 1605 Watchhill Rd, Austin, Texas 78703

(Received 28 June 2018; accepted 2 November 2018; published 20 November 2018)

The measurement of roughness of small lithographic patterns is biased by noise in the scanning electron microscopes (SEMs) used to make the measurements. Unbiasing the roughness measurement requires the measurement and subtraction of the image noise based on its unique frequency behavior. Improvement to prior white noise removal is achieved by applying a pink noise model. This pink noise removal technique was applied to roughness measurements made with different electron doses (frames of integration), different operating voltages, and different generations of SEM tools. Effective noise removal to create accurate unbiased estimates of the roughness was achieved over a wider range of SEM tool parameter settings than has been previously achieved. As a result, unbiased roughness measurements can now be used to characterize and improve stochastic variability in semiconductor lithography and patterning. *Published by the AVS.*

<https://doi.org/10.1116/1.5046477>

I. INTRODUCTION

Patterning for semiconductor manufacturing (lithography followed by etch) inevitably produces rough features due to the stochastic nature of the processes at nanoscopic length scales. Over time, Moore's law has dictated dramatic decreases in the dimensions of the features being printed, but the amplitude of the roughness on the edges of these features has shrunk only very slowly. As a result, the roughness of the edges as a fraction of the feature size has grown to the point where stochastic-induced feature roughness is now one of the major concerns for semiconductor patterning at the 10-nm node and below. Stochastic effects can reduce the yield and performance of semiconductor devices in several ways: within-feature roughness can affect the electrical properties of a device, such as metal line resistance and gate leakage; feature-to-feature size variation caused by stochastics [also called local critical dimension (CD) uniformity] adds to the total budget of CD variation, sometimes becoming the dominant source;^{1,2} feature-to-feature pattern placement variation caused by stochastics (also called local pattern placement error) adds to the total budget of pattern placement errors, sometimes becoming the dominant source;³ rare events in the tails of the distributions of errors are more probable if those distributions have fat tails, leading to greater than expected occurrence of catastrophic bridges or breaks;⁴ decisions based on metrology results (including tool and material selection, process optimization, process monitoring and control, and the calibration of lithography models) can be poor if those metrology results do not properly take into account stochastic variations.

For these reasons, proper measurement and characterization of stochastic-induced roughness is critical. Unfortunately, current roughness measurements [such as the measurement of linewidth roughness (LWR) or line-edge roughness (LER) using a critical dimension scanning electron microscope

(CD-SEM)] are contaminated by large amounts of measurement noise caused by the CD-SEM. This results in a biased measurement, where the true roughness adds in quadrature with the measurement noise to produce an apparent roughness that overestimates the true roughness. Furthermore, these biases are dependent on the specific CD-SEM tool used and its settings, as well as on the feature being measured. Attempts to reduce noise in the SEM image often involve filtering of the image, which can reduce bias (generally by an unknown amount) but adds further uncertainty to the measurement.

In a previous study, a new technique for producing unbiased estimates of roughness parameters was investigated.⁵ It is based on the use of an analytical model for SEM scattering behavior that predicts linescans for a given feature geometry. Run in reverse, an inverse linescan model can be used for edge detection in such a way that SEM noise can be adequately measured and statistically subtracted from the roughness measurement, thus providing unbiased estimates of the roughness parameters. The previous study investigated the impact of pixel size/magnification and number of measurement frames averaged (i.e., electron dose) on the measured roughness. In this study, a given sample set (with given roughness characteristics) will be measured under a variety of CD-SEM conditions: different SEM voltage and multiple CD-SEM tools. Furthermore, efforts to better measure roughness at very low electron doses will be tested. Ideally, each of these measurement tool settings will only have negligible impact on the unbiased roughness measurements, even though they are known to have a significant impact on biased roughness measurement.

II. IMPACT OF NOISE ON ROUGHNESS MEASUREMENT

The biggest impediment to accurate roughness measurement is noise in the CD-SEM image. SEM images suffer from shot noise, where the number of electrons detected for

^{a)}Electronic mail: chris.mack@fractilia.com

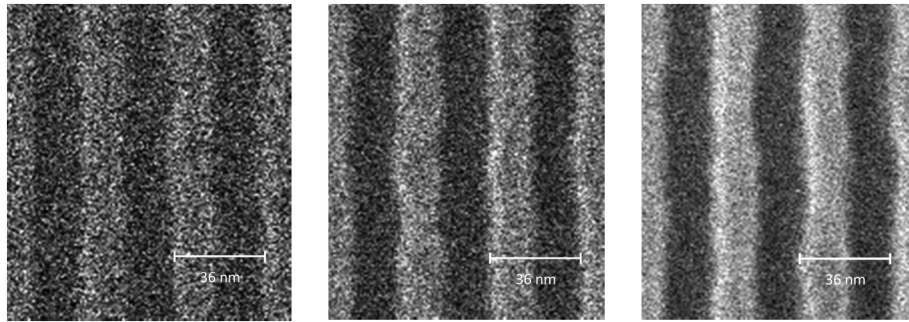


FIG. 1. Portions of SEM images of nominally identical resist features with 2, 8, and 32 frames of integration (respectively, from left to right). Doubling the frames of integration doubles the electron dose per pixel. Since the dose is increased by a factor of 4 in each case, the noise goes down by a factor of 2. Reprinted from Chris A. Mack, *J. Micro/Nanolithogr. MEMS MOEMS* **17**, 041006 (2018). Copyright 2018, Society of Photo Optical Instrumentation Engineers.

a given pixel varies randomly. For the expected Poisson distribution, the variance in the number of electrons detected for a given pixel of the image is equal to the expected number of electrons detected for that pixel. Because the number of detected electrons is proportional to the number of electrons that impinge on the sample location represented by that pixel, the relative amount of noise can be reduced by increasing the electron dose from the CD-SEM that the sample is subjected to. For some types of samples, electron dose can be increased with few consequences. But for most samples (especially photoresist), high electron dose leads to sample damage (resist line slimming, for example⁶). Thus, to prevent sample damage, electron dose is kept as low as possible, where the lowest dose possible is limited by the noise in the resulting image. Figure 1 shows portions of three SEM images of nominally the same lithographic features taken at different electron doses.⁷

SEM image noise adds to the actual roughness of the patterns on the wafer to produce a measured roughness that is biased higher⁸

$$\sigma_{\text{biased}}^2 = \sigma_{\text{unbiased}}^2 + \sigma_{\text{noise}}^2, \quad (1)$$

where σ_{biased} is the roughness measured directly from the SEM image, σ_{unbiased} is the unbiased roughness (that is, the true roughness of the wafer features), and σ_{noise} is the random error in the detected edge position (or linewidth) due to noise in the SEM imaging and edge detection. Because an unbiased estimate of the feature roughness is obviously what is desired, the measured roughness must be corrected by subtracting an estimate of the noise term.

Pixel noise in the SEM creates edge detection noise depending on the shape of the expected linescan for the feature. For example, Fig. 2 shows a typical linescan (grayscale value g vs horizontal position x), perpendicular to a line feature on a wafer, when there is an extremely large number of electrons so that the pixel noise is negligible. The result is the “expected” linescan, that is, the expectation value of the linescan signal from a statistical perspective. By defining a threshold grayscale level, the edge position can be determined by the intersection of the linescan with the threshold (Fig. 2). But noise in the grayscale values results in

noise in the detected edge position. For a given grayscale noise σ_{gray} , the edge position uncertainty σ_{noise} will depend on the slope of the linescan at the edge dg/dx . For small levels of noise and a continuum grayscale signal,

$$\sigma_{\text{noise}} \sim \frac{\sigma_{\text{gray}}}{dg/dx}. \quad (2)$$

Thus, the level of edge detection noise is a function of the pixel grayscale noise and the slope of the linescan at the feature edge.

Equation (2) is strictly only valid for small levels of noise and an infinitely small pixel size. To explore the impact of greater amounts of noise and a nonzero pixel size, simulation of SEM images was employed.⁹ Perfectly smooth lines and spaces (25 nm width, 50 nm pitch) were used as inputs to the analytical linescan model¹⁰ in order to create synthetic SEM images. Then, the grayscale values (which range from 0 to 255) of each pixel were varied using a normal distribution as an approximation to the Poisson distribution, with a variance proportional to the mean grayscale value. By specifying the grayscale noise (σ_{gray}) at a grayscale value of 128 (the midpoint of the range), the input to the normal distribution random number generator at a mean grayscale value of g is then

$$\sigma_{\text{normal}}(g) = \sigma_{\text{gray}} \sqrt{\frac{g}{128}}. \quad (3)$$

The impact of image noise on detected edge noise depends on the method of edge detection. To study this effect, these synthetic SEM images were treated as experimental SEM images and measured using a simple threshold model with no image

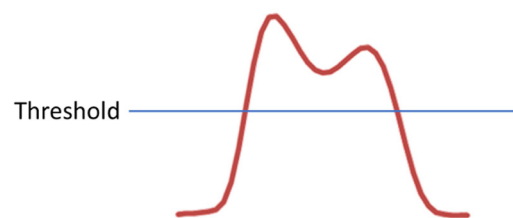


FIG. 2. Detecting an edge from a linescan (grayscale value vs horizontal position) with no noise.

processing and using the Fractilia inverse linescan model (FILM) (using the software program MetroLER, v1.6.5) to detect the edge positions of each feature. The 1-sigma LER measured from these images is the detected edge position uncertainty due to grayscale pixel noise (since the true LER is zero). Because the inverse linescan modeling uses data from the entire linescan to find the edge position,¹¹ its edge detection variation in the presence of noise is reduced from that of the simple threshold model as described by Eq. (2).

Figure 3(a) shows that the FILM edge detection is more robust in the presence of noise than a threshold edge detection, with a lower sensitivity to grayscale noise. When the grayscale noise is sufficiently high, the threshold edge detector tends to detect the noise rather than the edge. On the other hand, the impact of grayscale noise on the FILM edge detection noise is close to linear. Furthermore, smaller x pixel sizes (Δx) produce lower levels of edge detection noise [Fig. 3(b)]. In fact, the simulated edge detection variance σ_{noise}^2 is directly proportional to the x pixel size

$$\sigma_{\text{noise}}^2 \approx k \Delta x \left(\frac{\sigma_{\text{gray}}}{255} \right)^2, \quad (4)$$

where in this case, $k = 21$ nm (a measure proportional to one over the grayscale slope of the expected linescan) for the data from Fig. 3(b).

The importance of the scaling relationship above becomes apparent when considering noise removal from the roughness

power spectral density (PSD). Given the grid size along the length of the line (Δy), SEM edge detection white noise biases the PSD according to¹²

$$\text{PSD}_{\text{biased}}(f) = \text{PSD}_{\text{unbiased}}(f) + \sigma_{\text{noise}}^2 \Delta y. \quad (5)$$

Because σ_{noise}^2 is directly proportional to Δx for the case of FILM edge detection, the noise floor will be proportional to $\Delta x \Delta y$, the area of one pixel. For a square pixel, that means the PSD noise floor is proportional to the pixel size squared.

In order to effectively measure and subtract out noise, the noise floor must be sufficiently smaller than $\text{PSD}(0)$ (the low frequency plateau of the PSD) so that it can be estimated using a reasonable number of SEM images. For M features (or edges) averaged together, the relative random uncertainty (one standard deviation) of the PSD at a specific frequency will be $1/\sqrt{M}$.¹² For 400 features, the LWR PSD will have a $\pm 5\%$ uncertainty (1σ). A good rule of thumb might be that the unbiased $\text{PSD}(0)$ must be greater than the noise floor [the biased $\text{PSD}(0)$ must be twice the noise floor]. If $\text{PSD}_{\text{unbiased}}(0) = 2\sigma_{\text{LER}}^2 \xi$ (where ξ is the roughness correlation length), combining with Eq. (4) gives

$$2\sigma_{\text{LER}}^2 \xi > k \left(\frac{\sigma_{\text{gray}}}{255} \right)^2 \Delta x^2, \quad (6)$$

$$\Delta x < \frac{\sigma_{\text{LER}}}{\sigma_{\text{gray}}/255} \sqrt{\frac{2\xi}{k}}. \quad (7)$$

The importance of Eq. (7) is mostly as a scaling relation. As roughness (σ_{LER}) decreases, the measurement pixel size should scale with the roughness and with the square root of the correlation length. Also, higher levels of grayscale noise require smaller pixel sizes to achieve the same ratio of signal to noise in the PSD.

The noise constraint of Eq. (7) on the x pixel size should be coupled with the requirement of small y pixel size relative to the correlation length in order to properly detect the noise floor. A good rule of thumb for this constraint is that $\Delta y < \xi/5$. For extreme ultraviolet lithography processes, we

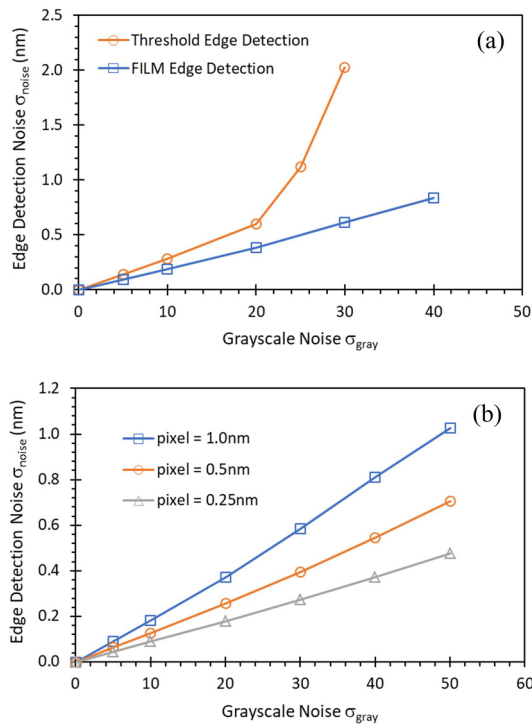


Fig. 3. Edge detection noise as a function of grayscale noise for simulated synthetic SEM images (average of 100 images, each with 20 dense lines/space features of width 25 nm) with added grayscale noise: (a) the FILM is less sensitive to grayscale noise as compared to a threshold edge detector and (b) smaller pixel sizes produce less edge detection noise (using FILM) for a given pixel grayscale variation.

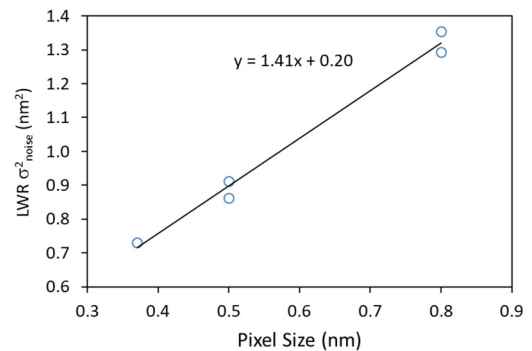


Fig. 4. Edge detection noise variance as a function of pixel size for the measurement of 16 nm resist lines and spaces on a Hitachi CG5000 CD-SEM tool. Square pixels were used.

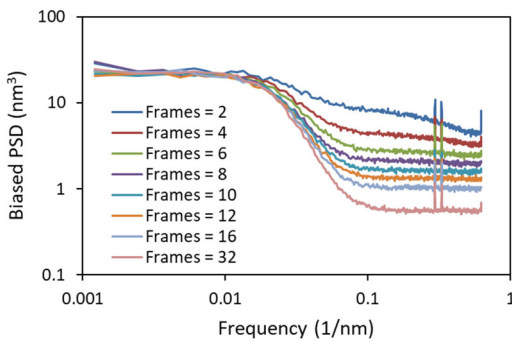


FIG. 5. Power spectral densities (PSDs) of 18 nm resist lines and spaces where only the number of frames of integration was varied. SEM conditions: 500 eV, 49 images per condition, 21 features per image, pixel size = 0.8 nm square, image size = 1024×1024 pixels. Reprinted with permission from Gian F. Lorusso *et al.*, *Microelectron. Eng.* **190**, 33 (2018). Copyright 2018, Elsevier.

typically find correlation lengths between 5 and 10 nm so that y pixel sizes should be kept at 1 nm or below.

Poisson pixel noise is not the only source of edge detection noise. Beam current instability will add pixel noise that is not Poisson. During operation, the electron beam is scanned from left to right using beam steering electronics. Errors in the beam steering can place the beam at an incorrect position, which produces an edge error. Charging of the sample during electron exposure will deflect the beam to an incorrect position. While much of the charging effects will be systematic, there will also be random or pseudorandom components that will appear as random variation in the detected edge position.

To validate the above simulation results, both the magnification and the pixel size were varied experimentally on a Hitachi CG5000 CD-SEM tool. These two parameters can be changed independently by changing the number of pixels in the image (between 512×512 and 2048×2048). Square pixel sizes were 0.37, 0.50, and 0.80 nm, with two magnifications used for the 0.5 and 0.8 nm pixel cases. Figure 4 shows the measured edge detection noise for a pattern of 16 nm lines and spaces for different magnifications

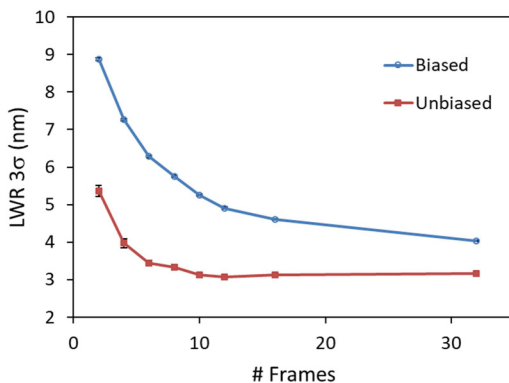


FIG. 6. Biased and unbiased measurements of 3σ LWR as a function of the number of frames of integration. All conditions were the same as described in Fig. 5. Error bars represent 95% confidence interval estimates. Reprinted with permission from Gian F. Lorusso *et al.*, *Microelectron. Eng.* **190**, 33 (2018). Copyright 2018, Elsevier.

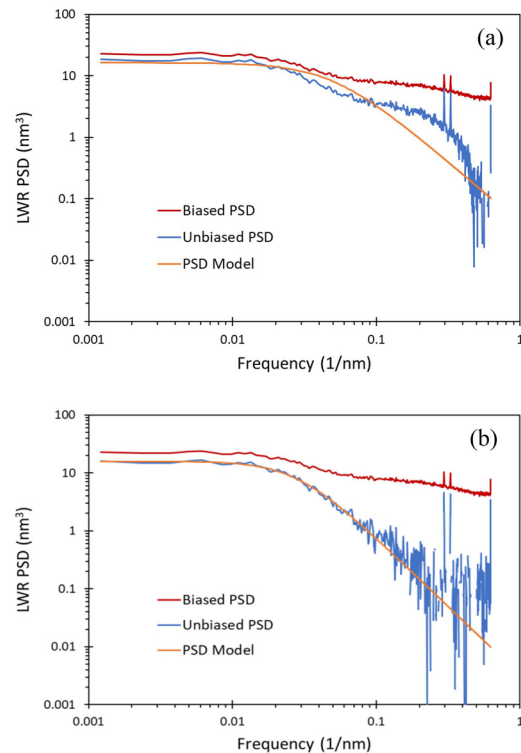


FIG. 7. Using the biased PSD data from Fig. 5 for the case of two frames of integration, (a) white noise only subtraction vs (b) pink noise subtraction. For pink noise subtraction, the resulting unbiased PSD follows the expected shape at mid to high frequencies.

and pixel sizes. The dose per pixel was kept constant so that the electron shot noise is expected to be independent of pixel size. In fact, the grayscale noise in each image was measured to be 32.3 ± 0.2 for the five images. Consistent with the simulation results, edge detection noise variance was linear with the pixel size (and though not shown, the PSD noise floor was also linear with pixel size squared). The offset (intercept) in the trend indicates edge detection noise that is independent of pixel size and is thus probably from a source other than grayscale noise. Clearly, the majority of edge detection noise is coming from pixel noise induced errors, with the value of k from Eq. (4) equal to 11 nm.

III. WHITE NOISE VERSUS PINK NOISE

While Eq. (5) shows the impact of white noise on the roughness PSD, not all SEM noise in measured PSDs is white noise. White noise occurs when the measurement

TABLE I. Difference between white noise removal and pink noise removal for the data shown in Fig. 7.

	White noise removal	Pink noise removal
3σ unbiased LWR (nm)	5.18 ± 0.07	3.73 ± 0.12
PSD(0) (nm^3)	16.27 ± 0.85	15.88 ± 0.35
Correlation length (nm)	3.19 ± 0.23	5.70 ± 0.17
Roughness exponent	0.5	0.69 ± 0.06

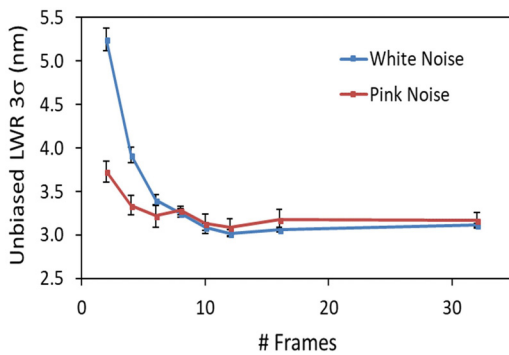


Fig. 8. Using the biased PSD data from Fig. 5, the resulting unbiased LWR 3σ estimates as a function of the number of frames of integration for both white noise and pink noise removal. Ideal behavior would be a flat line as a function of number of frames. Error bars represent 95% confidence interval estimates.

noise of the edge position from each linescan is completely independent of all other linescans (and in particular, its nearest neighbors). White noise occurs in the absence of correlations that connect the errors in one linescan row to the errors in the neighboring linescans. Any small correlations in edge errors along the length of the line would cause “pink noise,” a noise signature that is not perfectly flat over the entire frequency region.

In a previous study, the impact of various SEM metrology tool settings on the unbiased roughness was investigated.⁵ One parameter studied was the number of frames of integration, which was varied from 2 to 32, representing a $16\times$ variation in SEM electron dose. Figure 5 shows PSDs of 18 nm resist lines and spaces measured with different frames of integration on a Hitachi CG5000 CD-SEM. The cases of eight or more frames of integration exhibit a fairly flat high-frequency noise region. For two and four frames of integration, the noise region is noticeably sloped. Thus, the assumption of white SEM noise is only approximately true and becomes more accurate as the noise level decreases. This observation has been borne out in other circumstances: high noise cases (and low contrast images) are more likely to exhibit nonflat noise floors.

Figure 6 shows the biased and unbiased values of the 3σ linewidth roughness measured as a function of the number of frames of integration under the assumption of white noise. The biased roughness varies from 8.83 nm at 2 frames of integration to 5.68 nm at 8 frames and 3.98 nm at 32 frames.

The unbiased roughness, on the other hand, is fairly stable after 6 frames of integration, varying from 5.25 nm at 2 frames of integration to 3.25 nm at 8 frames and 3.11 nm at 32 frames. While the biased roughness is 43% higher at 8 frames compared to 32, the unbiased roughness is only 4% higher at 8 frames compared to 32. Since the assumption of white SEM noise is not very accurate at two and four frames of integration, the noise subtraction of the unbiased measurement using a white noise model is not completely successful at these very low frames of integration.

One potential cause of correlations in edge noise would be correlations in the pixel noise. To test this possibility, isolated edges were measured in the CD-SEM. The edge allows the SEM to perform its imaging functions in a typical way, but at a distance left or right from the edge, the image field is flat and featureless. In this region, the only variation in pixel grayscale values comes from image noise. The correlation coefficient between neighboring pixels can then be calculated. Performing these calculations, the average correlation between neighboring pixels in the x -direction (the scanning direction) was 0.12–0.16. These correlation coefficients were determined for edges measured at 2–32 frames of integration, with the correlation coefficient rising about 25% from a low of 0.12 at 2 frames of integration to 0.16 at 32 frames of integration. In the y -direction, the correlation between pixels was only about 0.01, essentially zero. From these results, it is easy to conclude that correlated pixel noise is not responsible for the pink noise observed at low frames of integration.

It is possible that the linescan slope in Eq. (2) is responsible for the noise correlations. As the linewidth and space-width of a small feature change along the length of the feature, the linescan slope will change as well. Variations in the linescan slope will cause edge detection error similar to grayscale variations among pixels. If these linescan slope changes are independent from one row of pixels to the next, the result will be white noise. But this may not be the case. When electrons enter the sample at a specific point, the material interaction volume of the electrons can be from a few to a few tens of nanometers in diameter, depending on the beam voltage and the sample material properties. This interaction volume means that electrons impinging on one spot on the sample are influenced by the sample shape over a range determined by the interaction volume. Thus, the slope of the linescan at one row of pixels will not be independent of the slope of the linescan at neighboring pixels whenever

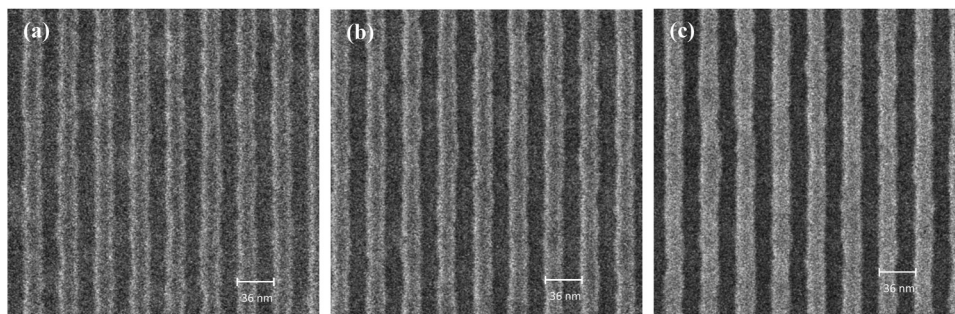


Fig. 9. Samples of SEM images of resist 18 nm lines and spaces for (a) 300 V, (b) 500 V, and (c) 800 V operation of the CD-SEM (8 pA current, 16 frames).

the interaction volume radius is greater than the y pixel size. This dependency could be the cause of correlations in the noise, with a noise correlation length affected by the electron beam interaction volume.

IV. REMOVING PINK NOISE FROM A POWER SPECTRAL DENSITY

The model for white noise is a flat (constant) PSD of the noise, which adds to the PSD of the feature roughness equally over all frequencies. For pink noise, a more complicated noise model is required. The key to determining a reasonable model for pink noise is to recognize the role of correlations in the noise signature. Like roughness itself, correlations in noise reduce the noise at high frequencies (those higher than the frequency corresponding to the correlation length of the noise). Thus, a PSD model for pink noise will be similar to a PSD model for the roughness itself: flat (white) at low frequencies, transitioning to fractal (sloping downward) at length scales below some correlation length. This correlated noise model can then be added to a white noise model to create the final pink noise model. In many cases, the low frequency noise level is not much different from the high-frequency noise level so that a simple white noise model is sufficient.

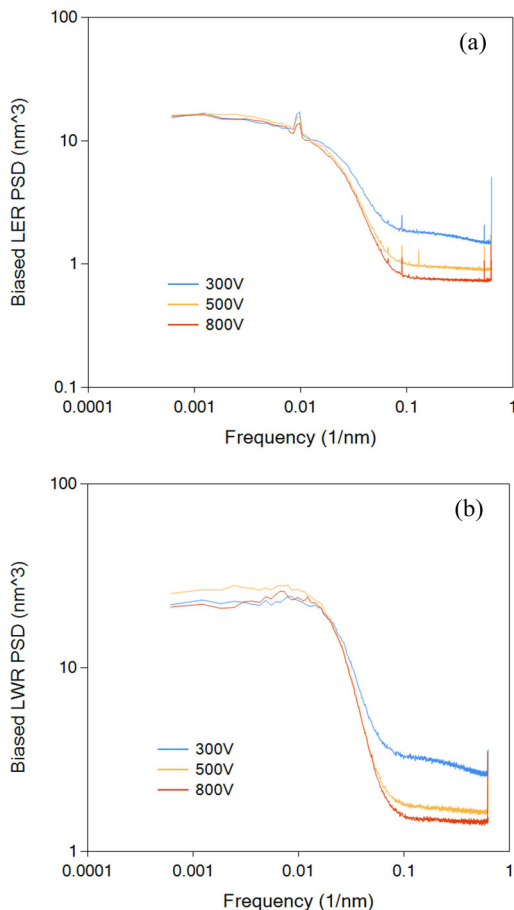


FIG. 10. Biased PSDs (before noise removal) as a function of voltage: (a) LER, the average of left and right edges, and (b) LWR.

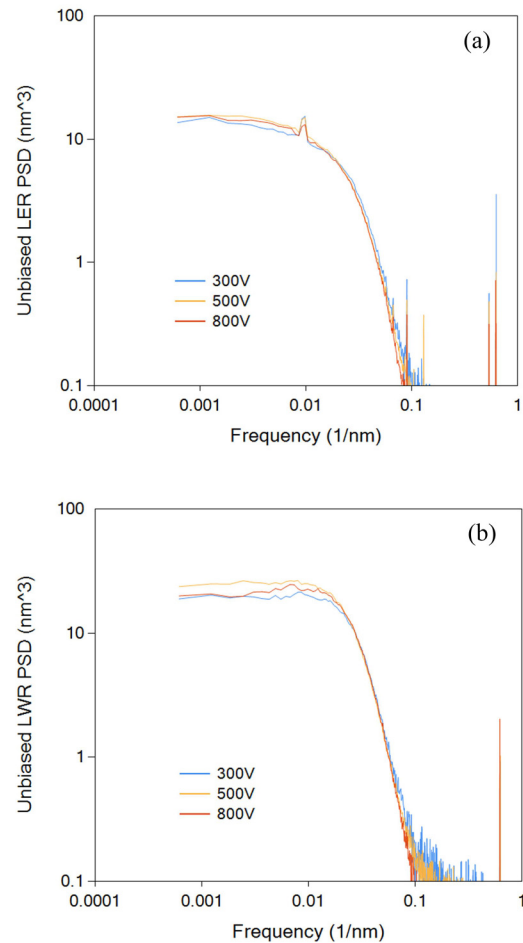


FIG. 11. Unbiased PSDs (after noise removal) as a function of voltage: (a) LER, the average of left and right edges, and (b) LWR.

The difference between using a white noise model and a pink noise model can be seen in Fig. 7 and Table I for the case of the two frames of integration data from Fig. 5. The resulting unbiased PSD (after noise subtraction) follows the expected shape only for the case of pink noise subtraction. The difference in the extracted roughness parameters is quite significant when comparing white noise removal to pink noise removal (see Table I). For white noise removal, the unbiased PSD exhibits a shape quite different from the PSD model, making model fitting and parameter extraction potentially unreliable. For this case, the pink noise correlation length was approximately one half of the y pixel size.

The data from Figs. 5 and 6 can be used to explore the efficacy of the pink noise removal process. Figure 8 shows

TABLE II. LER results (average of left and right edges) as a function of voltage.

	300 V	500 V	800 V
Biased 3-sigma (nm)	4.93 ± 0.01	4.04 ± 0.01	3.74 ± 0.01
Unbiased 3-sigma (nm)	2.52 ± 0.09	2.46 ± 0.01	2.35 ± 0.02
PSD(0) (nm ³)	13.01 ± 0.21	14.72 ± 0.19	13.90 ± 0.17
Correlation length (nm)	8.01 ± 0.16	9.07 ± 0.16	8.98 ± 0.15
Roughness exponent	0.68 ± 0.04	0.72 ± 0.03	0.71 ± 0.03

TABLE III. LWR results as a function of voltage.

	300 V	500 V	800 V
Biased 3-sigma (nm)	6.63 ± 0.02	5.60 ± 0.01	5.30 ± 0.01
Unbiased 3-sigma (nm)	3.49 ± 0.05	3.57 ± 0.02	3.40 ± 0.03
PSD(0) (nm ³)	19.93 ± 0.07	25.68 ± 0.08	22.40 ± 0.13
Correlation length (nm)	5.88 ± 0.02	6.70 ± 0.02	6.13 ± 0.04
Roughness exponent	1.40 ± 0.02	1.30 ± 0.02	1.46 ± 0.04

the estimated unbiased LWR as a function of the number of frames of integration for both pink noise and white noise removal. Ideally, every measurement would produce the same unbiased LWR value to within measurement uncertainty since the true roughness on the wafer is a constant. As can be seen in Fig. 8, pink noise subtraction does a better job of providing an unbiased LWR estimate over a wider range of frames of integration. In particular, the two, four, and six frames data produce much better unbiased roughness

estimates using the pink noise model. For example, for the case of 4 frames of integration compared to 32 frames of integration, white noise subtraction produces an estimate that is 26% too high, whereas pink noise subtraction produces an estimate that is only 5% too high (within the measurement uncertainty for this experiment).

V. CD-SEM VOLTAGE

SEM voltage has a complicated impact on the measured linescan. Generally, a higher voltage produces a less noisy image but has the potential for greater sample damage, especially for photoresist. It is not uncommon to use a lower voltage for measuring the roughness of resist lines and a higher voltage for measuring the roughness of after-etch lines. CD-SEM voltages between 300 and 800 V are commonly used, but the impact of voltage on the measurement of roughness, and in particular unbiased roughness, has not been thoroughly explored.

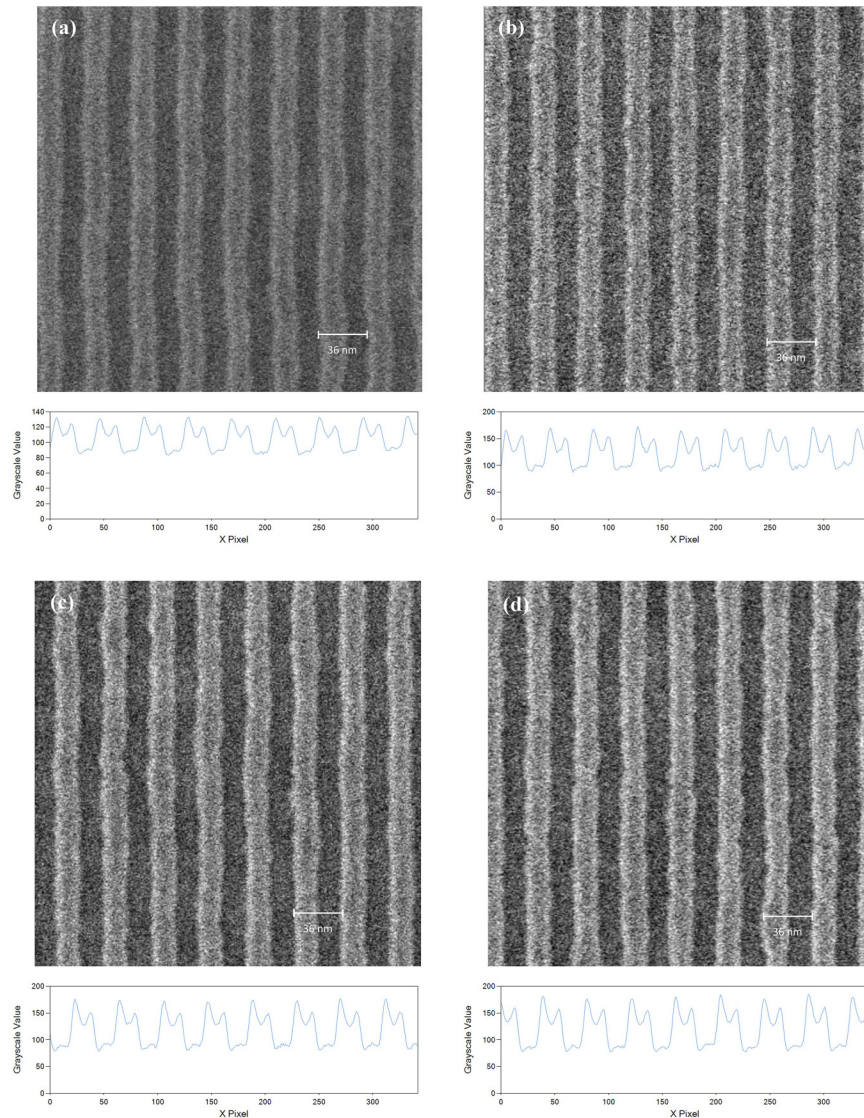


FIG. 12. Samples of SEM images of resist 18 nm lines and spaces for different Hitachi CD-SEM tools: (a) S-9380, (b) CG4000, (c) CG5000, and (d) CG6300. Below each SEM image is its average linescan, the average grayscale value of each column of pixels in the image.

Here, the voltage on the Hitachi CG5000 CD-SEM was set to 300, 500, and 800 V to measure photoresist features of nominally 18 nm lines and spaces. Three representative portions of SEM images are shown in Fig. 9. If the only impact of voltage is on the noise in the image, the hope is that proper noise removal from the PSD will enable accurate measurement of the roughness (including all PSD parameters) for each of these voltages.

Figures 10 and 11 show the PSDs (biased and unbiased, respectively) resulting from the measurement of 103 images, each 2048×2048 pixels using 0.8 nm square pixels (thus averaging together 4466 lines that are each 1630 nm long). For the calculation of the 300 V unbiased PSDs, the pink noise removal approach described above was used. Summary results are also given in Tables II and III (for LER and LWR, respectively), showing the biased and unbiased 3σ roughness and the unbiased PSD parameters as a function of voltage.

From both the graphs and the tables, we can see that the biggest difference in the biased roughness as a function of voltage comes from the noise, and that the noise removal process does a fairly good job of removing the noise and erasing most of the differences as a function of voltage. The biased 3σ LER varies by 28% across voltage, while the unbiased 3σ LER varies by 7%. The 3σ LWR shows a similar improvement (22% variation for the biased roughness,

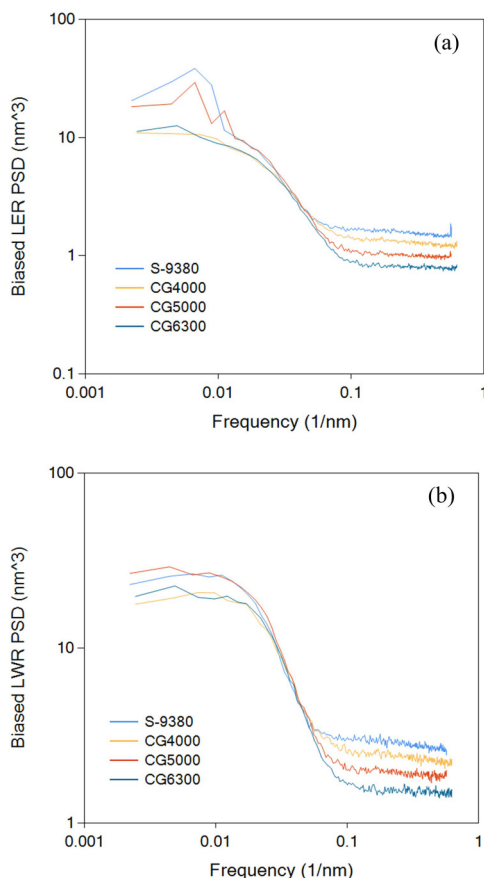


FIG. 13. Biased PSDs (before noise removal) as a function of tool set: (a) LER, the average of left and right edges, and (b) LWR.

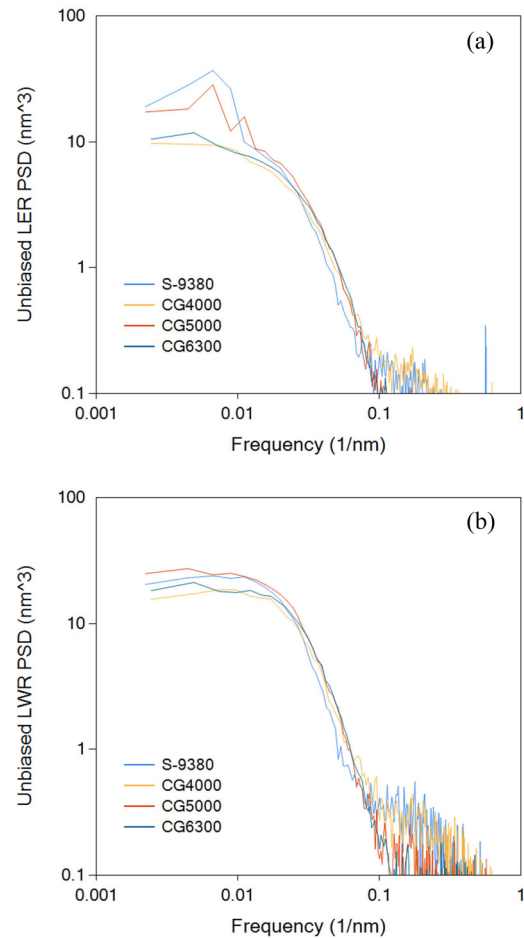


FIG. 14. Unbiased PSDs (after white noise removal) as a function of tool set: (a) LER, the average of left and right edges, and (b) LWR.

decreasing to 5% for the unbiased LWR), though with more variation in the PSD(0) values than seen for the LER.

VI. CD-SEM TOOL SET

The final study compares results from four generations of CD-SEM tools from Hitachi (listed from oldest to newest): S-9380, CG4000, CG5000, and CG6300. The newer tools are much more flexible in terms of magnification, pixel size, and numbers of pixels per image. Thus, finding a common tool setup for comparison purposes that could be replicated on every tool meant being limited by the capabilities of the oldest tool. The chosen setup used 512×512 pixels, 0.88 nm

TABLE IV. LER results (average of left and right edges) as a function of CD-SEM tool set.

	S-9380	CG4000	CG5000	CG6300
Biased 3-sigma (nm)	4.73 ± 0.02	4.32 ± 0.02	4.14 ± 0.02	3.71 ± 0.02
Unbiased 3-sigma (nm)	2.63 ± 0.07	2.25 ± 0.03	2.66 ± 0.03	2.21 ± 0.02
PSD(0) (nm ³)	35.85 ± 3.48	9.99 ± 0.21	24.32 ± 2.91	10.85 ± 0.38
Correlation length (nm)	14.94 ± 1.46	8.05 ± 0.22	12.56 ± 1.88	8.06 ± 0.37
Roughness exponent	1.03 ± 0.03	0.65 ± 0.04	0.63 ± 0.17	0.65 ± 0.06

TABLE V. LWR results as a function of CD-SEM tool set.

	S-9380	CG4000	CG5000	CG6300
Biased 3-sigma (nm)	6.25 ± 0.03	5.99 ± 0.04	5.66 ± 0.03	5.24 ± 0.03
Unbiased 3-sigma (nm)	3.42 ± 0.04	3.30 ± 0.04	3.60 ± 0.04	3.27 ± 0.04
PSD(0) (nm ³)	23.84 ± 0.31	18.36 ± 0.31	25.74 ± 0.27	19.24 ± 0.27
Correlation length (nm)	6.83 ± 0.09	6.06 ± 0.11	6.57 ± 0.08	5.79 ± 0.09
Roughness exponent	1.36 ± 0.06	1.14 ± 0.06	1.15 ± 0.04	1.22 ± 0.06

square pixel size (for a line length of 450 nm), 500 V, 16 frames of integration, and a current between 7.2 and 8.5 pA. Measurements were made on photoresist features of nominally 18 nm lines and spaces. Representative portions of SEM images are shown in Fig. 12, along with average linescans (averaging all pixel grayscale values in each vertical column of pixels).

PSDs for LER and LWR before and after noise subtraction are shown in Figs. 13 and 14 (the average of 102 images, each with 11 lines and spaces). The oldest tool, the S-9380, exhibits an anomalous bump in low frequency LER (absent in the LWR) that can be seen as a wiggle of the lines in the SEM image. The CG5000 tool exhibits a spike in the LER at a frequency of about 0.006 nm⁻¹ (corresponding to a length of about 150 nm, or about 1/3 of the frame height) and its harmonic, while the LWR does not show such a spike. A possible explanation for the spike (and possibly for the bump in the S-9380 LER data) is electrical interference in the beam steering electronics periodically shifting entire pixel rows of the beam. It should be noted that the spikes seen in the CG5000 LER PSDs come and go in various data sets indicating intermittent interference.

Biased and unbiased 3 σ roughness and unbiased PSD parameters are shown in Tables IV and V for the LER and LWR, respectively. The results in the tables confirm the visual interpretation of the PSDs. Unbiasing the results produces a better match between tools, but differences remain due to the wiggle and spikes found in the S-9380 and CG5000 tools. For both LER and LWR, the CG4000 and CG6300 unbiased results match extremely well.

VII. CONCLUSIONS

The primary goal of metrology is to produce accurate measurements. Accuracy is difficult to assess in an absolute sense for roughness metrology due to a lack of verified roughness standard measurement artifacts, but the *lack* of accuracy in a measurement is obvious whenever measurement results change with the arbitrary setting of metrology tool parameters. For the measurement of roughness in a CD-SEM, there are a number of tool settings that have no obvious “right” value but nonetheless can dramatically change the measured value: the combination of pixel size

and magnification (number of pixels per image), electron dose (current and number of frames of integration), voltage (landing energy), and measurement tool model. Additionally, image processing settings (part of an edge detection algorithm) such as filter/smoothing parameters and the threshold value used for edge detection can also affect the results. There is, however, an obvious correct setting for the use of filtering: none (all filtering/smoothing turned off).¹³ The use of inverse linescan modeling for edge detection was employed in this work to enable robust edge detection without the use of filtering, with the added benefit of making the results independent of the edge detection threshold value.¹¹

This work carries on a previous effort⁵ to look at the four sets of CD-SEM parameters mentioned above to access the accuracy of roughness metrology. We have shown that bias in the roughness measurements caused by SEM noise can vary (sometimes dramatically) as a function of pixel size, electron dose, SEM voltage, and SEM tool. By unbiasing the measurements (measuring and subtracting out the SEM noise contribution to the results), a stable result can be obtained that is mostly or wholly independent of these tool settings. The main conclusions of this effort so far are first that unbiased measurements are independent of pixel size so long as the y pixel size is small compared to the roughness correlation length and the x pixel size is small enough to enable an acceptable signal to noise ratio. Unbiased roughness is independent of electron dose (frames of integration) down to moderately small dose levels using white noise removal and down to extremely small dose levels using pink noise removal. Measurements of resist features using voltages between 300 and 800 V produce images with significantly different noise levels, but unbiasing the results can remove most of these differences. Finally, different CD-SEM tools also have different noise levels but become comparable when the noise is removed. Some tools, however, can exhibit anomalies in the LER PSD, probably due to electrical interference.

Further work could explore the sources and behaviors of some of the observed inaccuracies. What are the sources of PSD spikes/wiggle and what can be done to eliminate them? How do changes in the y pixel size affect pink noise? What other factors might affect pink noise (such as the linescan slope)? This study has brought us close to our ultimate goal: accurate roughness measurements. Further study could bring us closer.

¹R. L. Bristol and M. E. Krysak, *J. Micro/Nanolithogr. MEMS MOEMS* **16**, 023505 (2017).

²Fuming Wang, Stefan Hunsche, Hung Yu Tien, Peng Tang, Junwei Wei, Yongjun Wang, Wei Fang, and Patrick Wong, *J. Micro/Nanolithogr. MEMS MOEMS* **17**, 041007 (2018).

³Allen Gabor, Andrew Brendler, Timothy Brunner, Xuemei Chen, James Culp, and Harry Levinson, *J. Micro/Nanolithogr. MEMS MOEMS* **17**, 041008 (2018).

⁴Peter De Bisschop, *J. Micro/Nanolithogr. MEMS MOEMS* **17**, 041011 (2018).

⁵Gian F. Lorusso, Vito Rutigliani, Frieda Van Roey, and Chris A. Mack, *Microelectron. Eng.* **190**, 33 (2018).

⁶Benjamin Bunday et al., *Proc. SPIE* **7638**, 76381L (2010).

⁷Chris A. Mack, *J. Micro/Nanolithogr. MEMS MOEMS* **17**, 041006 (2018).

⁸Benjamin D. Bunday *et al.*, *Proc. SPIE* **5375**, 515 (2004).

⁹P. P. Naulleau and J. P. Cain, *J. Vac. Sci. Technol. B* **25**, 1647 (2007).

¹⁰Chris A. Mack and Benjamin D. Bunday, *Proc. SPIE* **9778**, 97780A (2016).

¹¹Chris A. Mack and Benjamin D. Bunday, *Proc. SPIE* **10145**, 101451R (2017).

¹²Chris A. Mack, *J. Micro/Nanolithogr. MEMS MOEMS* **12**, 033016 (2013).

¹³Gian Francesco Lorusso *et al.*, *J. Micro/Nanolithogr. MEMS MOEMS* **17**, 041009 (2018).